AVALANCHE FAILURE OF YARNS IN A 3D WOVEN COMPOSITE: FINITE ELEMENT MULTI-SCALE MODELLING BASED ON TOMOGRAPHY INSPECTION

L. Laiarinandrasana*[1], W. Trabelsi[1], A. Thionnet[2]

[1] *Centre des Matériaux, UMR CNRS 7633, Mines ParisTech, BP87, 91003 Evry Cedex, France*
[2] *Université de Bourgogne, Mirande, BP 47870, 21078 Dijon Cedex, France*
* *Corresponding Author: lucien.laiarinandrasana@mines-paristech.fr*

Keywords: Textile composite, Multi-scale analysis, Finite Element, Stress concentration coefficient

Abstract

The degradation of a textile composite was observed at the microscopic scale using the micro-computed tomography technique. All the warp yarns at the top surface were broken showing fracture surfaces perpendicular to the yarn's longitudinal axis. Finite element modelling taking these observations into account was perfomed. The results showed that the largest principal stress is the driving parameter leading to the damage mechanisms. According to the kind of applied load, the numerical simulation of warp yarn breakage based on this parameter led to a good prediction of the failure mechanisms: either in avalanche or progressive failure.

1. Introduction

Fiber reinforced composite materials such as textile composites exhibit complex architectures. The failure mechanisms appearing in those heterogeneous materials depend on in what occurs within the fabric reinforcement. The investigated textile composite is subjected to in-service cyclic bending combined with a small tensile load. This loading provokes degradation of the structure inducing a decrease of the stress at failure of the specimen. The early stage of yarns breakage cannot be detected at the macroscopic scale. But this is of prime importance for the assessment of the residual lifetime of the engineering structure, especially for an avalanche type failure. Indeed, laboratory tests under cyclic tensile loading resulted in an avalanche type failure of the warp yarns.

This work deals with a multi-scale analysis in terms of experimentation and finite element modelling. First, inspections of many degraded samples were carried out by using micro-computed tomography (μCT). These allowed a precise description of the map of the broken yarns within the structure. The localization of the broken yarns as well as the orientation of fracture's surfaces are respectively detailed. Finite element modelling was then motivated by the abovementioned observations. A periodic cell with an adapted fine meshing in the critical sections was designed. Two boundary conditions were considered: fully tensile and combined bending with light tensile loadings. The mechanical analysis allowed for a better understanding of the state of damage on the one hand and for a prediction of the the failure mechanisms of the textile

composite on the other hand.

2. Experiments

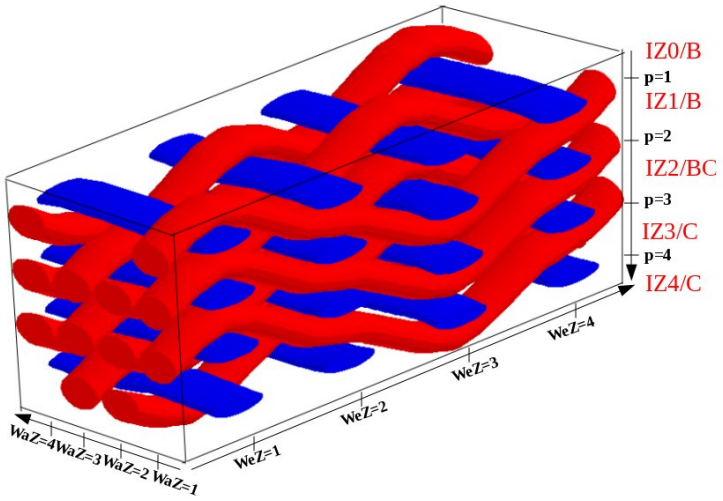

Figure 1. Nomenclature for 2.5D angle interlocked woven fabric under study

The composite material under investigation is a 2.5D angle interlocked woven fabric [1, 2, 3]. The matrix, the warp and the weft yarns are respectively made of polyvinylchloride (PVC), polyethylene terephtalate (PET) and polyamide 66 (PA66). Figure 1 details the architecture of such a fabric for which a precise nomenclature was given in order to better understand the localization of the damage in the sequel. The weft yarns are straight whereas the warp yarns are undulating over a number of weft yarns. In fig. 1, the definition of both warp zones (WaZ) and weft zones (WeZ) was reported in [4]. Here attention is paid to the interzones (IZ): the (straight) weft yarns allow the determination of 4 horizontal planes. These planes mark out the 5 volumes called IZ i ($i \in \{0, 1, 2, 3, 4\}$). IZ0 being the "top" IZ: the first IZ from the top surface of the composite material. Within each IZ the warp yarn can have various configurations according to its position in the undulation:

- Ascendent (A) when the segment of warp yarn presents a positive angle with respect to the horizontal plane
- Bump, noted "B" corresponds to the peak position on the undulated warp yarn (convex shape);
- "C" is related to the bottom position of the undulation (concave medium line of the warp yarn)
- Descendent (D) corresponding to the opposite of (A) geometry

In fig. 1 IZ0/B deals with the first IZ (number 0) from the top surface within which the warp yarns are composed of only "B" segments. What occures in this IZ0B is of prime importance in the sequel. Furthermore, in the present architecture, the same warp yarn has its "B" configuration in IZ0 and its "C" configuration in IZ2. Indeed IZ2 is the interzone of symmetry, containing both "B" and "C" configurations. Focus will then put only on IZ0/B, IZ1/B and IZ2/B.

As already reported in previous work [3], a degraded sample previously subjected to in-service cyclic bending/tensile load exhibited: i) regularly periodic "bumps" at the top surface of the material; ii) a significant decrease in the stress at failure of the degraded textile composite. To better understand the degradation phenomena, laboratory tests were carried out under fully tensile cyclic loading. For the highest maximum stress level applied, the specimen was broken after about 10^3 cycles. This latter case showed a brittle fracture of the composite material, that is a failure in avalanche of the warp yarns. An attempt was made here to analyze the cause of the change in the kinetics of yarn breakage. To this end, experimental investigations at the macroscopic and mesoscopic scales were performed.

2.1. Critical stress concentration coefficient

Tensile tests were carried out on individual warp yarns as well as on the textile composite laminate. The stresses at failure σ_R and Σ_R for the warp yarn and for the composite laminate respectively were determined from these tensile tests. It should be noted that the failure of tested specimens occured in a brittle manner without any apparent necking. It can then be assumed that these stresses at failure were obtained whilst under uniaxial stress state. In the following, the analysis is essentially based on σ_R, that is, the composite laminate is supposed to initiate its failure process as soon as σ_R is reached in any warp yarn. This concept allowed the introduction of a critical stress concentration coefficient K_σ^C [3, 2] defined as follows:

$$K_\sigma^C = \frac{\sigma_R}{\Sigma_R} \tag{1}$$

K_σ^C is specific to this fabric with its constituents. The security in-service of the composite is ensured if the stress concentration coefficient –*the ratio between a local stress in the warp yarn and the global stress applied to the woven fabric*– is less than K_σ^C, provided that these latter stresses are **uniaxial**.

2.2. Micro Computed Tomography inspections

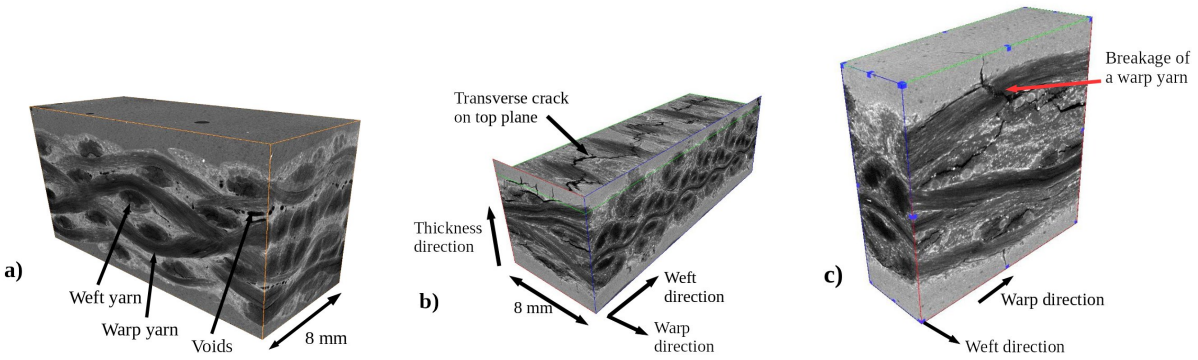

Figure 2. μCT volumes of of the textile composite: a) the initial microstructure; b) a degraded material; c) breakage of a warp yarn

Micro-computed tomography (μCT) is a non destructive technique delivering images in 3D of the damaged microstructure. Figure 2 illustrates some reconstructed images from both as-received (fig. 2a) and degraded specimens (fig. 2b-c). Fig. 2a, reveals manufacturing defects such as porosity, microcracks networks in the matrix and yarns' misalignement. Fig.2b depicts

a top view of transverse cracks (through width) crossing the PVC matrix as well as the warp yarns in their the peak positions "B": this plane belongs to IZ0B interzone. By focusing on one particular warp yarn, it can be observed in fig. 2c that, on the one hand, the crack appears in the peak of undulation of each warp yarns; on the other hand, crack surfaces are perpendicular to the yarn axis. These observations were obtained on all warp yarns in IZ0/B whereas no warp yarn was broken in the other IZ's (IZ1-4). This information about the localization and the orientation of the cracks is of prime importance for this engineering component subjected to in-service cyclic bending/tensile loading.

3. Finite Element modelling

3.1. Meshes, boundary conditions and constitutive models

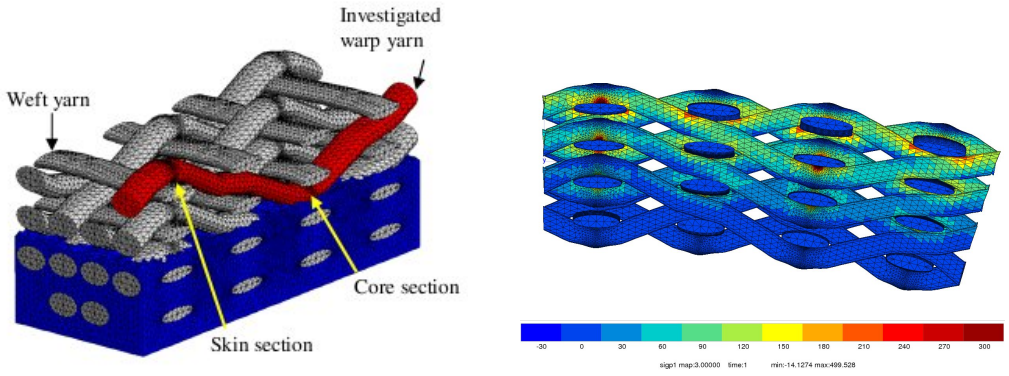

Figure 3. a) Meshes of the periodic cell; b) σ_{p_1} contour map for combined tensile/bending loading

FE simulations were carried out using linear elastic behaviours: the matrix and the yarns were assumed to be respectively isotropic and orthotropic. The local Euler angles within each yarn were updated during the computation in order to fit to the orthotropic conditions. A 3D periodic cell was determined from the textile composite architecture (fig. 3a). The meshes consisted of 591,209 tetrahedral linear elements, with 312,105 degrees of freedom. In the upper part of the mesh, the matrix was removed in order to show the yarns arrangement. Mesh refinements were operated around the section on "B" and "C" segments of warp yarn. The aim was to better analyze the stress and strain distributions in these sections.

Two kinds of loading were applied to this periodic cell: tensile and combined bending/tensile loadings. The first one deals with the experimental results from laboratory tests, concerning cyclic tensile loading (avalanche failure). The latter case is related to the in-service loading on the real structure that resulted in the damaged microstructure description in section 2.2 (fig. 3b). The prescribed boundary conditions were such that the stress in the warp yarn in IZ0/B was equal to σ_R. This situation mimics the stress state in the materials just before the failure of one warp yarn.

3.2. Results and discussion

FE results on individual warp yarn were already reported in the previous works [2, 3, 4]. Figure 3b illustrates, for instance the contour map of the largest principal stress σ_{p_1} in the periodic cell

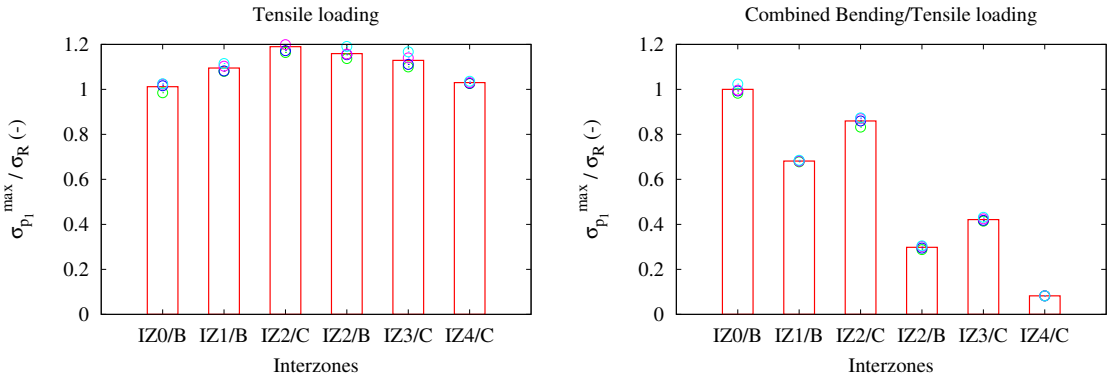

Figure 4. Normalized maximum principal stress distribution in the interzones

subjected to combined tensile/bending loading. σ_{p_1}, σ_{p_2} and σ_{p_3} are respectively the principal stresses ordered such that $\sigma_{p_1} \geq \sigma_{p_2} \geq \sigma_{p_3}$. It is then to be remembered that each warp yarn is subjected to an uniaxial stress state corresponding to $\sigma_{p_2} = \sigma_{p_3} \simeq 0$. Moreover:

- σ_{p_1} reaches its maximum value at "B" (and "C") configurations of the warp yarn;
- the eigenvector corresponding to σ_{p_1} systematically coincides with the normal to the fracture surface described in the section 2.2, that is, parallel to the yarn axis.

Let K_σ be the numerical stress concentration coefficient, defined as follows:

$$K_\sigma = \frac{\sigma_{p_1}^{max}}{\Sigma_{nom}} \tag{2}$$

where $\sigma_{p_1}^{max}$ and , Σ_{nom} are respectively the maximum value of the largest principal stress and the applied nominal stress at the macroscopic scale. It has been suggested that K_σ was the load parameter to be compared with K_σ^C previously introduced in section 2.1. Therefore, an efficient way to optimize the composite fabric consists of minimizing K_σ. From an engineering mechanics viewpoint, eq. (2) gives an access to the local stress $\sigma_{p_1}^{max}$. Indeed, knowing the applied global stress Σ_{nom} and the stress concentration coefficient K_σ, one can easily calculate $\sigma_{p_1}^{max} = K_\sigma \Sigma_{nom}$.

To go further, the abovementioned results were generalized to all warp yarns belonging to an interzone. To this end, for all warp yarns, figure 4 shows the variations of $\sigma_{p_1}^{max}/\sigma_R$ where σ_R is the stress at failure of an individual warp yarn determined in section 2.1. The two diagrams in fig. 4 illustrate respectively the tensile and the combined tensile/bending loadings. The histogram represents the average values of $\sigma_{p_1}^{max}$ in each IZ. The empty circle symbol corresponds to this stress value for a given warp yarn within the corresponding IZ. For IZ0/B, $\sigma_{p_1}^{max}/\sigma_R = 1$ due to the boundary conditions. The symbols clearly show that no variation was observed on $\sigma_{p_1}^{max}$ within each IZ. This means that as soon as one warp yarn is broken, all warp yarns of the corresponding IZ should break. Therefore, the analysis developed on individual warp yarn can be extended to the IZ: the breakage of all the warp yarns in an IZ is simultaneous.

This observation is not valid when analyzing the stress levels on all IZ's. Indeed, the bending load induces a gradient of $\sigma_{p_1}^{max}$ through the thickness of the laminate. IZ0 being the interzone where the maximum of $\sigma_{p_1}^{max}$ is reached. The stress gradient is clearly observed when considering separately "B" configuration and "C" one: either IZ0/B → IZ1/B → IZ2/B; or IZ2/C → IZ3/C → IZ4/C. Conversely, for the tensile loading the stress level in every IZ is roughly the same. This constant stress distribution is likely to induce an avalanche failure process from one IZ to another.

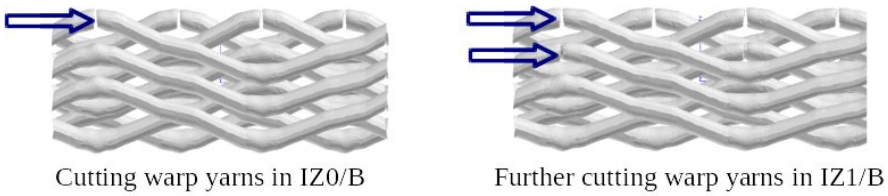

Figure 5. Meshes after incorporating fracture of warp yarns by IZ

So far, the simulations only show the stress states at the onset of the "initiation" of the warp yarn breakage within IZ0/B. An attempt is now made to numerically simulate the propagation of these warp yarn breakages, by incorporating IZ by IZ fractured warp yarns as detailed in fig. 5. The aim is here to evaluate the load ("stress") transfer between neighbouring warp yarns in consecutive IZ's. As mentioned previously, all warp yarns in IZ0/B have the same stress equal to σ_R; it is the first interzone where these warp yarns are broken at their peak position. The overstress observed in IZ1/B is considered as the load transfer in this configuration. The second series of "cuts" is operated in IZ1/B and the cumulative load transfer due to warp yarn breakages in IZ0/B and IZ1/B is evaluated in IZ2/C, and so on until IZ2/B.

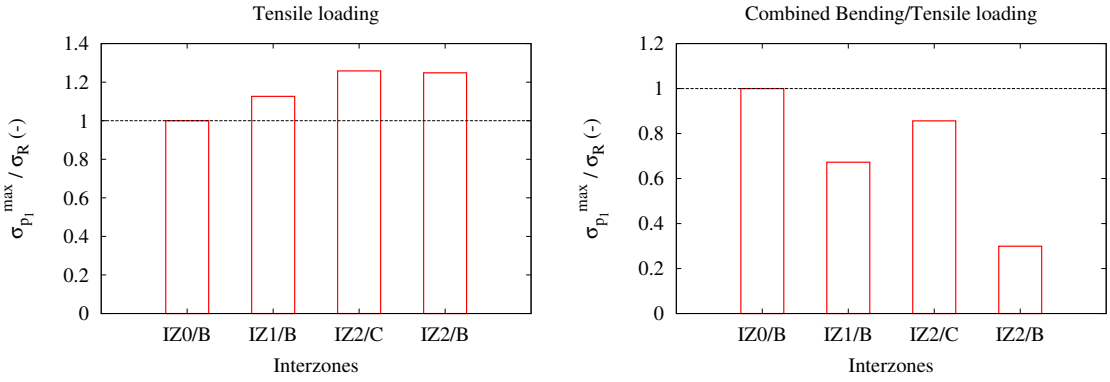

Figure 6. Evolution of $\sigma_{p_1}^{max}$ in each IZ after consecutive load transfers

The evolution of $\sigma_{p_1}^{max}$ with respect to the gradual breakage of warp yarns depends on the kind of loading. Under fully tensile load, the stress continuously increases - positive load transfer- so that the failure of warp yarns occurs obviously in an avalanche process. Conversely, under bending load, the gradual breakage of the warp yarns does not allow the stress to reach σ_R. Indeed, the load transfer is systematically negative or null in addtion to the gradient of stress established in the structure. Accordingly, although all warp yarns in IZ0 were cut, those in the other IZ cannot be broken. This distribution of stress induced by the load transfer, highlights

the observation of the microstructure in the degraded composite material (fig. 2.2) showing fractured warp yarns in uniquely IZ0/B. Moreover, because one IZ in 5 is broken, the stress at failure of this degraded specimen decreases with a magnitude of about 20% as measured experimentally.

4. Conclusion

During its service, the textile composite under study was subjected to a combined bending/tensile loading. A degraded sample exhibited periodic "bumps" at the top surface and an experimentally measured decrease in the stress at failure. By using micro-computed tomography (μCT) technique, a mapping of the damage at the microscopic scale was established. The warp yarns near the top surfaces were all broken whereas they were intact elsewhere in the architecture. Fracture occurred at the peak position of the undulation of the warp yarn, that coincided with the periodic bump observed at the macroscopic scale. Moreover, the fracture surfaces of these broken warp yarns turned out to be oriented perpendicularly to their longitudinal axis. Finite element modelling was performed to capture all of the abovementioned observations. Namely, it was shown that the maximum of the largest principal stress $\sigma_{p_1}^{max}$ played a major role to the local degradation mechanisms: it is located at the same place as the fracture within a warp yarn and the corresponding eigenvector is normal to the fracture surfaces. By determining the load transfer after consecutive breakage of warp yarns, it was shown that fully tensile load provokes failure in an avalanche process whereas combined bending/tensile led to a breakage arrest. These latter mechanisms explain better the observed damage mapping with μCT technique.

References

[1] B. Piezel, B. C. N. Mercatoris, W. Trabelsi, L. Laiarinandrasana, A. Thionnet, and T. J. Massart. Bending effect on the risk for delamination at the reinforcement/matrix interface of 3d woven fabric composite using a shell-like rve. *Composite Structures*, volume(94):2343–2357, 2012.

[2] W. Trabelsi, L. Laiarinandrasana, A. Thionnet, and S. Joannès. Durability of a 3d woven composite assisted by finite element multi-scale modeling. In *15th European Conference on Composite Materials (ECCM15)*. 2012.

[3] Laiarinandrasana, W. L. Trabelsi, and Thionnet. Finite element multi-scale modeling of the failure mechanisms in a 3d woven composite. In *19th International Conference on Composite Materials (ICCM19)*. 2013.

[4] W. Trabelsi. *Multiscale experimental and modelling approaches to predict the failure of a textile composite. Criteria for classification of woven fabrics*. PhD Thesis, Mines ParisTech, in French, Paris, 2013.